Hindawi
Advances in Civil Engineering
Volume 2021, Article ID 5580841, 16 pages
https://doi.org/10.1155/2021/5580841

Research Article

Performance of Pier-to-Pier Cap Connections of Integral Bridges under Thermal and Seismic Loads

Siva Avudaiappan,[1] **Kinson Prabu**,[2] **Deban Selvaraj**,[3] **Kiran Raja**,[4] **Paul Oluwaseun Awoyera**,[5] **and Erick I Saavedra Flores**[1]

[1]*Departamento de Ingeniería en Obras Civiles, Universidad de Santiago de Chile, Av. Ecuador 3659, Estación Central, Chile*
[2]*Structural Engineer, HCDA Engineering, Inc, Colorado Springs, CO, USA*
[3]*Indian Defense Accounts Secretary, Government of India, Chennai, India*
[4]*Project Planning Engineer, April-REG Group, Pangkalan Kerinci, Indonesia*
[5]*Department of Civil Engineering, Covenant University, Canaanland Ota, Ogun State, Nigeria*

Correspondence should be addressed to Siva Avudaiappan; siva.avudaiappan@usach.cl

Received 22 February 2021; Revised 25 June 2021; Accepted 29 July 2021; Published 11 August 2021

Academic Editor: Emanuele Brunesi

In general, most highway bridges are constructed using prestressed concrete or steel girders. Mechanical joints are provided at the end of each span, to allow for the expansion of the bridge deck due to shrinkage of concrete, thermal effects, and deflections, among others. Smooth riding ability, low noise, wear resistance, and water tightness should be provided by expansion joints. In recent times, the increased traffic volume, along with heavier vehicle movements, adversely affects the performance of expansion joints in the bridge girder, causing a possible failure in one of the above-mentioned mechanisms. The deterioration of the expansion joint may result in leakage of water, concrete cracking, and potential problems in the underlying substructure. In this paper, we study the pier-pier cap connections in integral bridges subjected to thermal and seismic loads using analytical methods and experimental tests.

1. Introduction

Integral bridges are constructed without joints or connection frames. These are characterized by a monolithic relation between the bridge deck and the substructure (piers and abutments). The intermediate connection between the two abutments is provided without any joints in the deck. Around the world, integral bridges have been built with different connection systems. These types of connections offer several advantages over simply supported bridges. The expansion joints and bearings provided in the simply supported bridge may lead to poor structural performance given the separation of the superstructure into two or more parts. Furthermore, integral bridges have a lower maintenance cost and lower corrosion issues when compared to bridges with expansion joints. The riding quality on the integral bridge is smoother. Moreover, redundancy is added to the structure by virtue of its monolithic property Holombo et al. [1] and Wassef et al. [2].

In spite of the relevance of integral bridge construction, there is still a lack of research on the analysis and design of integral bridge connections. For instance, in India, there are no standardized procedures for the design of integral bridge connections. Although engineers have developed guidelines based on the experience gained by conducting field tests and laboratory experiments, there are no proper guidelines, especially for the pier-pier cap connections. In particular, little attention has been paid to the thermal and seismic response of this type of connection. Therefore, in this paper, we investigate the behavior of integral bridges with pier-pier cap connections subjected to thermal and seismic loads.

The main novelties of the present research work are the following:

(1) Experimental investigation on the behavior of the connections of an integral bridge subjected to thermal and seismic loads

(2) Computational modeling of the above thermal and seismic behavior

(3) Validation of numerical predictions

The present paper is organized as follows. Section 1 introduces and reviews the main research works carried out in the context of integral bridges and their connections. Section 2 describes the experimental program followed in this paper. The casting details are detailed in Section 3. Section 4 gives information on the finite element modeling of the structure. The corresponding experimental results are given in Section 5. Section 6 presents the numerical results predicted by the computer model. The validation of the model is presented in Section 7. Finally, the main conclusions of this work are summarized in Section 8.

Abendroth and Greimann [3] carried out a research program to evaluate the design of integral abutment bridges using prestressed concrete (PC) elements and to validate the assumption of thermal loading conditions in the current design procedure for such types of connection in integral bridges. Over a period of two years, two skewed or bent PC girder integral abutment bridges were instrumented in order to test experimentally the structural behavior. Throughout the monitoring time, displacements, rotations, and temperature distributions along the longitudinal and transverse directions of the integral abutments were recorded for the PC girders. For different PC girders investigated under dry and saturated conditions, the concrete coefficients of thermal expansion and contraction were measured. Furthermore, the longitudinal displacements of the integral abutments were validated with experimental results obtained with changes in the bridge temperature. Such experimental data were utilized for the calibration of finite element models. The differences between the predicted and measured thermal expansions and vertical rotations of the bridge and integral abutments were not completely clarified.

Panday and Tandon [4] investigated the integral flyover at the intersection of Maa Anandamoyee Marg and Khegaon Marg on Outer Ring Road in Delhi and an intersection at Moti Nagar. A detailed study on the substructure and superstructure of the Kheagoan Marg Bridge was carried out. The superstructure was 150 m long with 5 spans, with a carriageway of 9 m and a depth of superstructure of 1.7 m. The substructure consisted of twin piers per carriageway per support location. Piers were rectangular with rounded short edges with a flute finish. The thermal load was decreased according to the stiffness and length of the structure, while the flexibility of the outer pier was gradually increased by the thickness from 1.15 m to 1.5 m. At the same time, the height of the pier was gradually increased from 0.5 m to 2 m at the base of the footing to the center of the structure. In this way, the flexibility was increased around 6 times at the end of the pier.

Laman [5] conducted a study on the superstructure stresses in prestressed girder integral abutment bridges by thermal induction. The stresses and forces were developed on the superstructure of prestressed concrete integral abutment bridges due to thermal loads. The loads applied on the superstructure showed a constant temperature change. Thermally induced superstructure forces were investigated on the bridge length, number of spans, abutment height, and pile orientation. Thermally induced superstructure stresses and forces reached maximum values near the abutment. It was found that the abutment height and bridge length highly influence the thermally induced superstructure forces. The thermally induced superstructure stresses were greatly influenced by the number of spans. The results showed that the thermally induced shear forces and superstructure stresses were comparable in magnitude to those produced by the live load.

Rodriguez Leo [6] monitored the temperature response of integral abutment bridges in Utah and California for approximately one year, using arrays of thermocouples through the height of girders and depth of the bridge deck. Temperature changes in concrete were recorded in addition to temperature gradients. A finite element model (FEM) was validated with the changes of deflections and strains monitored during a live-load test on the California Bridge and the changes of rotation observed from the thermal gradients of Utah Bridge. These results were used for the prediction of the bridge's internal stresses produced by temperature variations in the full cross section of the modeled bridge. Due to the measurements made on the end restraint of the California Bridge, it was found a very accurate prediction of its behavior at service conditions. The temperature differential and tensile stresses were obtained and correlated with the calculated values in concordance with design specifications.

Russell and Gerken [7] suggested design considerations for integral abutment bridges. It was noted that the movements occurred by changes in the bridge temperature and concrete creep and shrinkage, among others. They also suggested that the seasonal temperature changes affect the bridge length primarily, while the daily temperature affects the thermal gradients from the depth of the bridge structure.

Holombo et al. [1] conducted an experimental research on an integral bridge connection along its longitudinal direction. He prototyped two 40% scaled modeled bridges which represent the typical bridge construction in California. The columns were defined with an inelastic behavior, and the superstructure was designed to perform elastically. The test results showed a good ductility performance of the integral connection with a small strength degradation when subjected to seismic loads. The superstructure remained elastic with few small cracks, which closed after the removal of the corresponding loads. The author recommended extending the longitudinal reinforcement in the column as much as possible inside the bent cap to provide a better distribution of the seismic forces.

Chen et al. [8] conducted shake table tests on two 1/7-scale tall-pier models to evaluate the impacts of higher modes on the seismic performance of bridges with piers heights of over 40 m. They proposed two ways to improve the seismic performance: (1) eliminating the mid-height plastic response by including more longitudinal steel, and

(2) using more confinement in the mid-height region to improve pier ductility and avoid shear.

Mitoulis [9] conducted a review on the challenges and opportunities for the application of integral abutment bridges in earthquake-prone areas. The findings showed that backfill soil benefits the bridge mostly by reducing bending moments and pier drifts, which could lead to more cost-effective designs. However, because the IAB-backfill interaction was very case-dependent, careful and precise modeling of the backfill soil was suggested to avoid underestimating the bridge stresses.

Argyroudis et al. [10] conducted a research on the use of rubberized backfills for improving the seismic response of integral abutment bridges. The findings showed that using rubberized backfill reduces backfill settlements, bridge deck horizontal displacements, residual horizontal displacements of the top of the abutment, and abutment pressures by up to 55 percent, 18 percent, 43 percent, and 47 percent, respectively, when compared to a conventional backfill. On the abutment wall, there was also a noticeable reduction in bending moments and shear forces. As a result, rubberized backfills appeared to be a feasible alternative for reducing earthquake risk and achieving economic design goals for transportation network resilience with minimal damage.

Sritharan et al. [11] conducted an experimental investigation on an integral bridge pier consisting of a concrete column having *I*-shaped precast concrete girders with an inverted *T*-beam concrete cap, which accelerated the construction methods of the bridge in a seismic zone. The behavior of the overall system and girder-to-cap connections was evaluated. In the research, two girder-to-cap connections were analyzed: one was already implemented in practice and the other was a new proposed model. The research was conducted in a large-scale set-up, which helped to exhibit a good seismic response on the columns with successful plastic hinge formation. In the experimental study, the as-built connection with an inverted *T*-pier cap on an *I*-shaped precast girder behaved as a fully continuous connection rather than acting as a pinned connection. In the experiments, the improved girder-to-cap connections performed well, which showed a higher dependable response better than the as-built connection. Wang et al. [12] made an experimental investigation on the prefabricated bridge piers with grouted splice connections subjected to seismic loading. In his research, he found that the grouted splice piers performed better when compared to cast-in places. Grouted splice displacement capacity was lower than cast-in-place. Jia et al. [13] did their research on the precast bridge pier with elastomeric pads built-in subjected to seismic evaluation. In the research, elastomeric pads were kept at a plastic hinge area zone of the bridge pier. When subjected to seismic loads, the pier with the elastomeric pad showed better results. Usage of elastomeric pad provided stiffness and energy dissipation capacity. Zakeri and Zareian [14] made a design for a bridge with a skewed abutment subjected to minor earthquake loads. In his research, he found a negative trend present in between abutment skew angle and reliability index. He found that as the ratio of the column height to diameter increases, the reliability index becomes lower. His proposed method helped to design bridge piers for the target performance.

2. Experimental Program

The dimensions of a real bridge are taken and are reduced to one-fourth scale as per Cauchy's similitude law for fabrication of the experimental specimen. The bridge is modeled in STAAD. Pro and dead load, live load, and moments are determined as illustrated in Figure 1. Using the values obtained, the design and detailing of the bridge were carried out. Then, the materials are procured and the material properties are determined. The design mix for the M35 grade of concrete is carried out. Then, the reinforcement cage is prepared and strain gauges are attached to the specimens. Concreting and curing of the specimens are carried out and are then tested for thermal and seismic loads. Simultaneously, the structures are modeled in ANSYS 14.5, and the results of the loadings are obtained. Finally, the experimental and analytical results are compared and validated [15, 16].

2.1. Experimental Studies on Pier and Pier Cap Connections. The integral bridges are subjected to a variety of forces. These forces can be broadly classified into primary and secondary loads. The physical primary loads include live load, dead load, and seismic and wind loads, while the secondary loads are due to the sinking of supports, creep, and shrinkage, etc. Only a few secondary loads are significant in designing the structure. The cross section of deck and girders and IRC class-70R tracked and wheeled vehicle loading are illustrated in Figures 2 and 3, respectively [17–19].

To calculate the live and dead load moments and forces acting on the structure, the prototype is modeled and analyzed in STAAD.Pro. Loads are considered as per IRC class-70R loading.

The analysis of the prototype in STAAD.Pro is exhibited in Figure 4. The results obtained are as follows.

The total dead load and live load on the structure were 4300 kN and 980 kN, respectively. The pier cap is subjected to a factored bending moment of 6300 kN m and a factored shear of 2400 kN. The pier is subjected to a factored load of 7335 kN and a longitudinal moment of 1000 kNm and a transverse moment of 2740 kNm.

2.2. Description of the Bridge. The span of the prototype bridge is 60 m, in which the girder to girder distance is 3 m. The size of the pier cap is 1000 mm × 1600 mm and the size of the pier is 2000 mm × 800 mm. The taken model is 15 m, the girder to girder distance is 0.75 m, the size of the pier cap is 250 mm × 400 mm, and the size of the pier is 500 mm × 200 mm. The integral bridge has two lanes with a footpath on one end and a median on the other end. The specifications of the bridge and detailing of members of the bridge are presented in Tables 1 and 2, respectively. The dimensions of the bridge model and detailing of the pier, pier cap, and deck system of the bridge are illustrated in Figures 5 and 6, respectively.

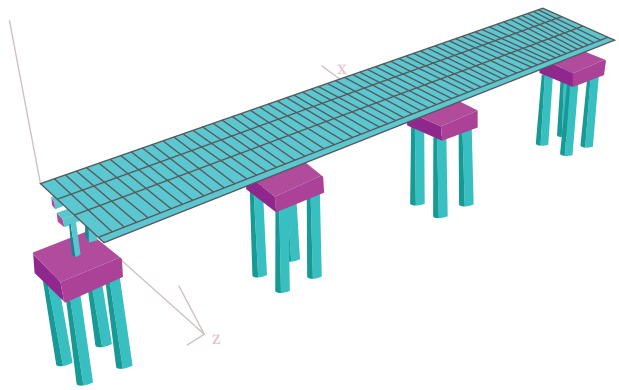

Figure 1: STAAD.Pro rendered view of the entire bridge.

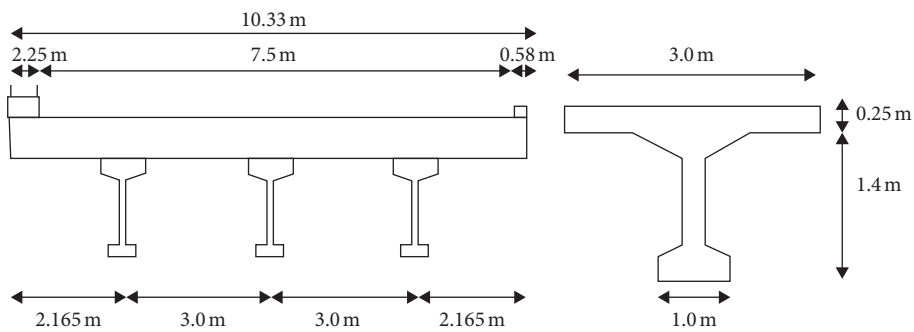

Figure 2: Cross section of deck and girders.

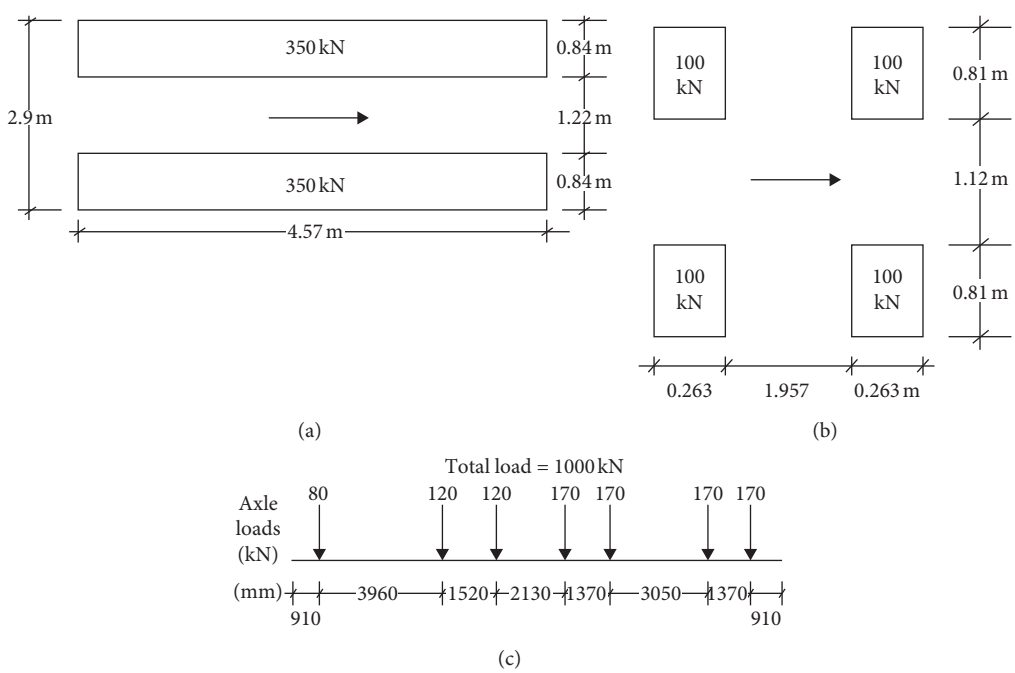

Figure 3: IRC class-70R tracked and wheeled vehicle loading.

2.3. Detailing. The bridge pier model that was used in the experiment is shown in Figure 6 with the reinforcement of bridge piers, pier cap, flexural, and shear reinforcement. The pier has 34 bars of 8 mm dia. and 128 bars of 6 mm dia., laterally and stirrups of 6 mm dia., with 62 nos. The anchor rod and the pier cap have 5 bars of 16 mm at the top and 5

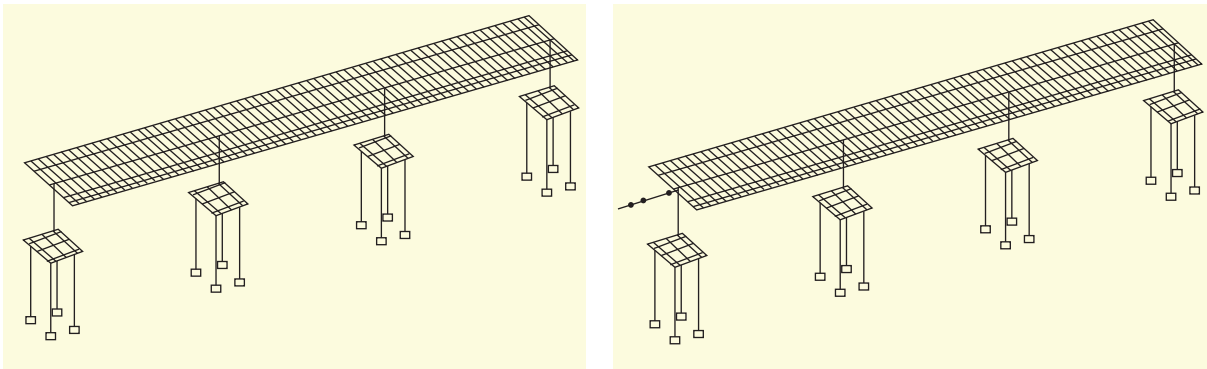

Figure 4: Modeling of the bridge in STAAD.Pro and determination of dead and live load acting on the pier, respectively, as per IRC class-70R loading.

Table 1: Specifications of the bridge.

Sl. No	Description	Prototype	Model
1	Span	60 m	15 m
2	Girder to girder distance	3 m	0.75 m
3	Pier cap	1000 mm × 1600 mm	250 mm × 400 mm
4	Pier	2000 mm × 800 mm	500 mm × 200 mm

Table 2: Details of members of the bridge.

Member	Longitudinal bars	Stirrups	Additional reinforcement
Pier	34 bars of 8 mm dia.	31 bars of 6 mm dia.	Anchor rods (1): 62 nos., of 6 mm dia., anchor rods (2): 128 nos., of 6 mm dia.,
Pier cap	5 bars of 16 mm at the top, 5 bars of 8 mm at bottom	19 bars of 6 mm two legged stirrups	Side face: 8 nos., of 6 mm, girder to pier cap:12# of 10 mm bars
Slab	30 bars of 10 mm dia.	22 nos., of 6 mm bars	

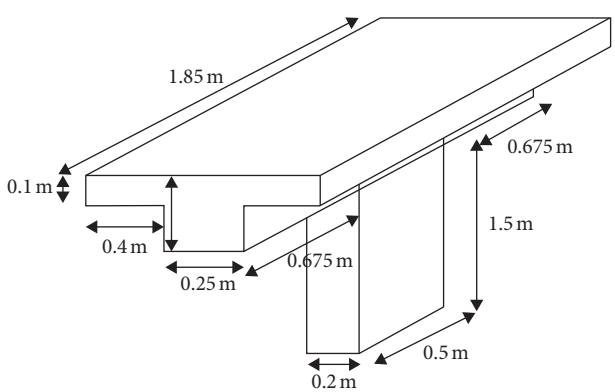

Figure 5: Dimensions of the bridge model.

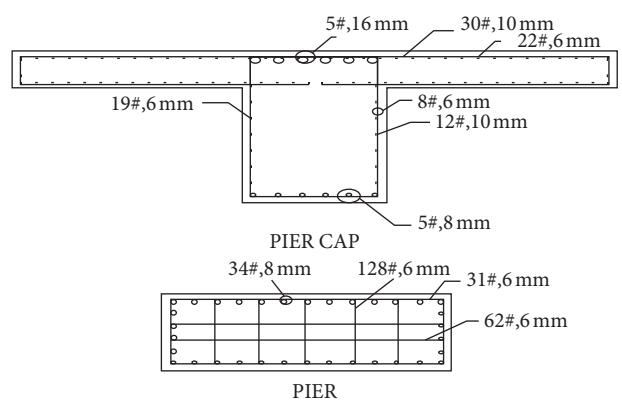

Figure 6: Detailing of the pier, pier cap, and deck system.

bars of 8 mm at the bottom. The slab is provided with 30 bars of 10 mm dia. There are main reinforcement and 22 numbers of 6 mm bar distributional reinforcement.

2.4. Material Properties and Design Mix. Materials were procured and tested in the laboratory to determine their physical properties, and their values are shown in Table 3. The cement used for the test is Ultra Tech Cement having a specific gravity of 3.15 g/cc and fineness modulus of 2.4. The coarse aggregate and fine aggregate were sieved as per IS 2386-1 (1963). The specific gravity of fine and coarse aggregate was 2.44 and 2.95, respectively. The fineness modulus of fine and coarse aggregate was 2.95 and 3.889, respectively.

The mix design for M35 concrete was determined as per [20], and the mix proportion is shown in Table 4. Sample cubes were cast and tested for their 28-day compressive

Table 3: Material properties.

Properties	Cement	Fine aggregate	Coarse aggregate
Specific gravity	3.159	2.44	2.95
Fineness modulus	2.4	2.784	3.889

Table 4: Mix proportions.

Water	Cement	Fine aggregate	Coarse aggregate
180 litres	400 kg	795 kg	1084 kg
0.45	1	1.9	2.7

strength. The average compressive strength of concrete was found to be 37.2 N/mm^2.

3. Specimen Casting

Based on the bar bending details, two reinforcement cages were prepared to test the behavior of pier-pier cap connections when subjected to thermal load and seismic loading, respectively. The strain gauges were positioned at the critical points in the reinforcement cage to measure the strain which will be experienced by the reinforcement at the time of loading. The critical sections were found from analysis of the structure in ANSYS 14.5 commonly used strain gauge consisting of an insulating flexible backing with a metallic foil pattern is used. The strain gauges attached to the reinforcement using adhesive are illustrated in Figures 7 and 8, respectively. When the reinforcement gets deformed, the foil also gets deformed, which makes the electrical resistance to change, which provides us the strain in a constant amount. The reinforcement cages are kept inside the mold, and the concrete is poured to obtain the desired shape and size of the specimen. The molds are made by using waterproof plywood (2 numbers of 7 × 4 feet and 1 number of 4 × 3 feet), and adequate supports are given at its sides which prevents the mold from deforming when concrete is poured. Runners were provided which avoids the bulging of the mold and the cover blocks of 20 mm are kept at its sides and bottom [21, 22].

The concrete mixture was mixed well in a batch mixer. The compaction was carried out using a needle vibrator, and the clogging was prevented by tamping of aggregates between the rebars to avoid honeycombing of structure. Segregation and bleeding of concrete have also been prevented while concreting the specimen. In each batch of specimen casting, 3 cubes were cast simultaneously. The specimen's demolding was carried out after 24 hours of curing. Water curing was done for 28 days by covering the specimen with fully soaked gunny bags. The details reinforcement and formwork for specimen are illustrated in Figures 9 and 10, respectively.

3.1. Experimental Set-Up and Loading. The experimental process was carried out in the Structural Dynamics Laboratory, Structural Engineering Division, Anna University.

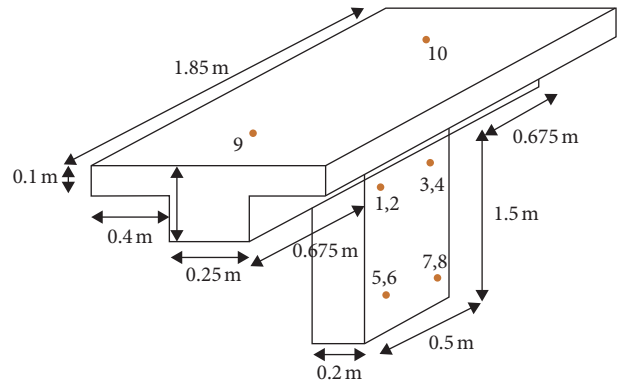

Figure 7: Location of the strain gauges.

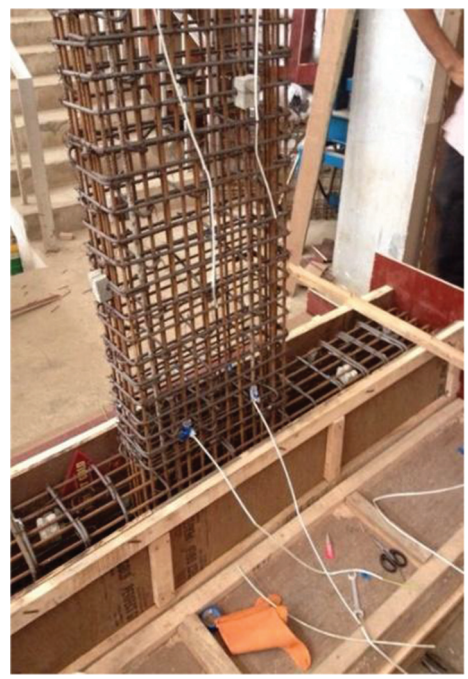

Figure 8: Strain gauge location in specimen 2.

The prototype specimens were tested in a well-equipped set-up which are subjected to thermal load and reverse cyclic loading. When applying the lateral loads, 50 kN capacity manual hand-controlled jacks were connected to the reaction frame, and the axial load was applied by using a hydraulic jack. The schematic view of the experimental set-up and testing of specimens for thermal load is illustrated in Figures 11 and 12, respectively.

The axial load was applied at the center of the pier. The slab was fixed to the frame to prevent rotation, and three plates were provided at the bottom of the slab, which induced internal stresses on the slab. For thermal analysis, the entire specimen was subjected to an axial load of 330 kN, and a lateral load of 11 kN was applied. For seismic analysis, an axial load of 280 kN (50% of the live load was considered as per codal provision) and a lateral load of 33 kN were applied.

Figure 9: Reinforcement cage of the specimen.

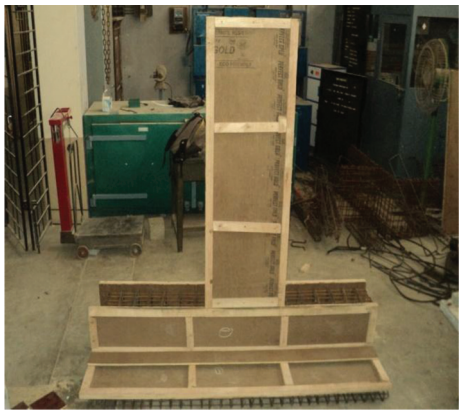

Figure 10: Formwork for the specimen.

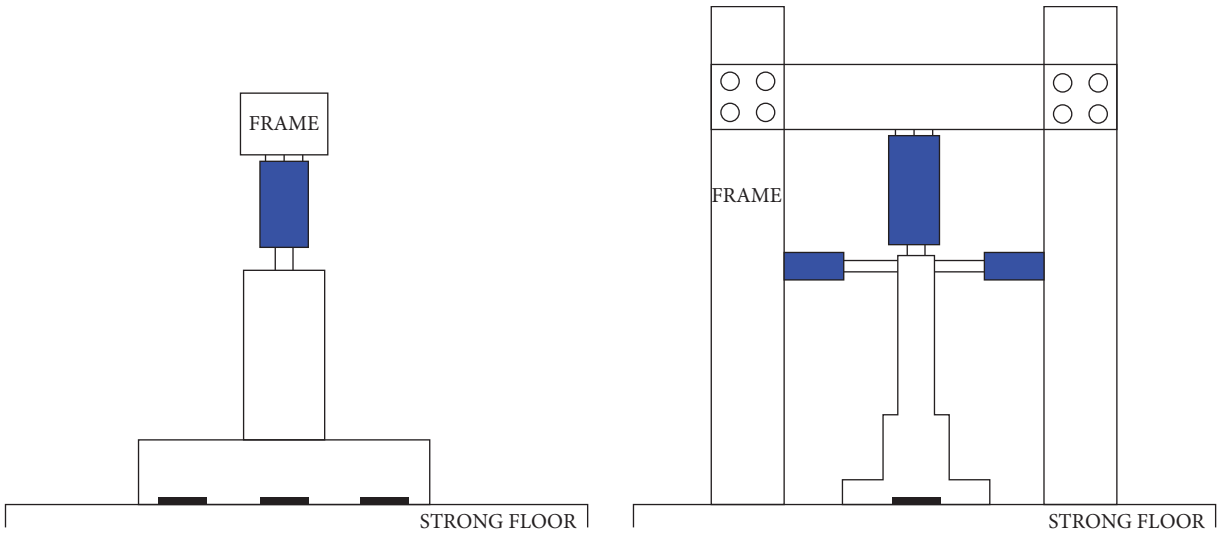

Figure 11: Experimental set-up (side view, front view).

Figure 12: Testing of specimens for the thermal load.

The lateral load of 11 KN was calculated from Hooks law $\Delta L/L = \alpha_L \Delta T$. This expression gives the stress for thermal analysis.

3.2. Testing of the Specimen. After the specimens were cast and cured for 28 days, they were moved to the strong floor using the gantry crane. The specimens were then centered and placed over three steel plates. Then, the specimens were tested for thermal and seismic loading.

3.3. Analytical Studies on Pier-Pier Cap Connections. Reinforced concrete structures have been largely deployed in various disciplines, especially in bridges. These structures are designed based on experimental data. Finite element analysis has provided a path for a more realistic analysis in various civil engineering disciplines including bridge structures. For instance, FEM provides a clear visualization of where the structure will twist or bend and indicates the distribution of displacements and stresses. Due to the complexity of the composite nature of the material, modeling structures is a challenging task.

The pier-pier cap joints of the integral bridge were modeled, analyzed, and designed in the previous sections. A scaled model was adopted for experimental investigation considering the testing facilities at the laboratory, and 1 : 4 scale was adopted. The same model was used for the analytical investigation.

4. Finite Element Modeling

The pier-pier cap model of 1/4th scale was analyzed using ANSYS software (version 14.5). Element type SOLID65 was selected to model the concrete. BEAM188 element was chosen to represent the reinforcement. SOLID65 was opted for the three-dimensional modeling of solids and reinforcing bars (rebars). The models of steel reinforcement and pier-pier cap are illustrated in Figures 13 and 14, respectively [23].

The solid65 has the capability of crushing in compression and cracking in tension. The elements were defined by eight nodes, each having 3 degrees of freedom with translations in the x, y, and z node directions. The BEAM188 element is relevant for analyzing the slender to moderately stubby/thick beam structures. The option BEAM188 is a 2-node linear element, whereas in 3D, it has 6 degrees of freedom at every node. The degrees of freedom in every node have the translations in x, y, and z directions and rotations in x, y, and z directions. The elements in the beams are suited for linear, large rotation, and large strain nonlinear applications. The real constants which are considered in SOLID65 elements are the volume ratio and the orientation angles in X and Y directions. The pier-pier cap model with discrete reinforcement was considered in the present study. As for the reinforcement, circular sections with the respective diameters were created, which were then imparted to the reinforcing element. BEAM188 and the steel properties were added in the element attributes window. The elements were then generated by creating and connecting the nodes.

4.1. Material Properties. The average cube strength (fck) at 28-day was 37.2 MPa, and it was used in modeling as obtained from the experiment. The elasticity modulus of concrete was considered as $5000\sqrt{\text{fck}}$ as per [24] which is $3.0414 \times 1010\ \text{N/m}^2$. Typical shear transfer range coefficients are from 0 to 1, in which 0 represents a smooth crack and 1 represents a rough crack. The uniaxial crushing stress used in the model refers to the uniaxial unconfined compressive strength. The uniaxial tensile cracking stress in concrete was determined by using the equation $f = 0.623\sqrt{\text{fck}}$ where fck is the cube strength of the experimentally tested specimen [25]. The material properties defined in the model are presented in Table 5.

4.2. Boundary Conditions

4.2.1. Displacement Boundary Conditions. The pier was assumed to be fixed at the slab in 3 lines; that is, all DOFs were constrained to simulate the presence of girder loads.

4.2.2. Load Boundary Conditions. In thermal analysis, the pier-pier cap connection was subjected to a pressure load of 330 kN at the base of the pier and the thermal lateral load was applied in increments up to 11 kN along the longitudinal direction of the pier. In the seismic analysis, the connection was subjected to an axial load of 280 kN at the base of the pier, and seismic loading is applied using reverse cyclic loading, applied in increments up to 33 kN along the longitudinal direction of the pier. The corresponding boundary conditions are illustrated in Figure 15.

The method of finite element analysis was carried out for pier-pier cap connection. The standard Newton-Raphson method was adopted for static analysis.

5. Experimental Results

5.1. Thermal Results. The bridge pier system in the inverted position was subjected to an increasing axial load up to 330 kN. The axial compression was simultaneously measured using LVDT. After the axial load reached 330 kN, an

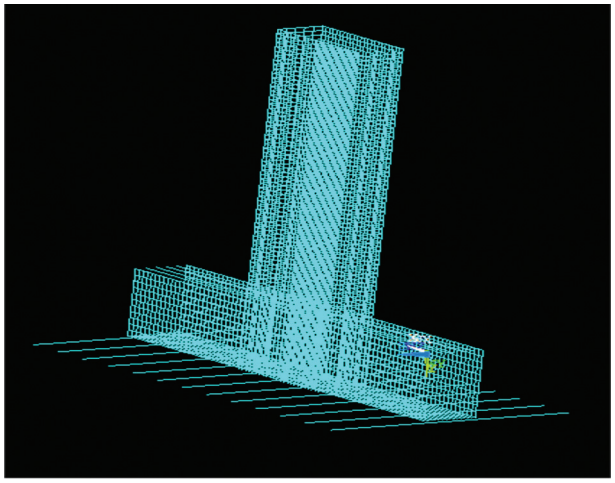

Figure 13: Steel reinforcement.

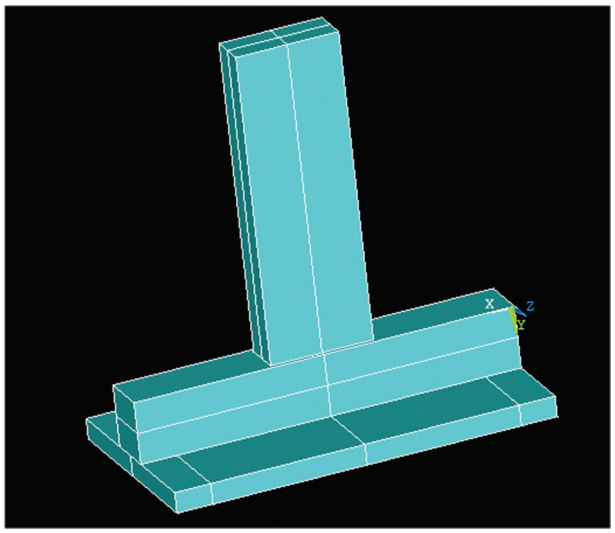

Figure 14: Pier-pier cap model.

Table 5: Material Properties defined in the model.

Material model no.	Element type	Material properties	
1	Solid65	Linear-elastic-isotropic	
		Young's modulus	3.0414×10^{11} N/m^2
		Poisson ratio	0.15
		Nonlinear- inelastic- von Mises criteria- concrete	
		Shear transfer coefficient for open crack	0.2
		Shear transfer coefficient for closed crack	0.9
		Uniaxial tensile cracking stress	3.71×10^6 N/m^2
		Uniaxial crushing stress	3.5×10^7 N/m^2
2	BEAM188	Linear isotropic	
		Young's modulus	2.1×10^{11} N/m^2
		Poisson's ratio	0.3
		Bilinear kinematic	
		Yield stress	4.1×10^8 N/m^2
		Tangent modulus	847×10^6 N/m^2

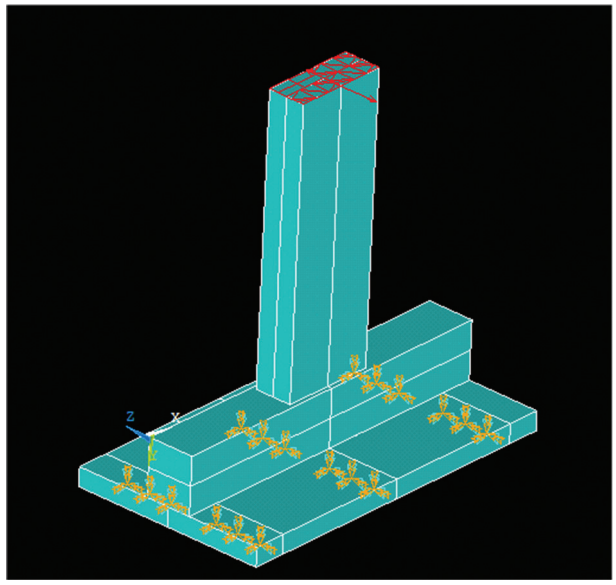

Figure 15: Boundary conditions.

increasing load up to 20 kN was applied by a manual hydraulic Jack fitted to the load frame. The lateral displacements were also measured for each 1 kN increment in load. The load was increased to 20 kN, to check for its lateral load-carrying capacity. The load versus displacement and axial stress versus axial strain are illustrated in Figures 16 and 17, respectively.

The axial stress versus strain of the specimen when subjected to thermal load is shown in Figure 17.

5.2. Seismic Type (Cyclic Loading) Results. For simulating the seismic effects, the specimen was subjected to the reverse cyclic loading of incremental loading up to 33 kN in an increment of 3 kN. The loading pattern is shown in Figure 18.

The lateral displacement was measured for each 3 kN increment in load. The lateral displacement with respect to load cycles is shown in Figure 19.

The lateral displacement versus lateral load graph is shown in Figure 20. It is seen from the graph that the curve is linear and the behavior is elastic.

6. Numerical Results

6.1. Thermal Results. With the application of thermal lateral load, the following displacement results are obtained. The displacement is found to be minimum at the slab and progressively increases toward the base of the column. The maximum displacement is found to be 3.67 mm. The displacement due to thermal loads is shown in Figure 21.

The stress accumulations due to the application of thermal loads are shown in Figure 22. The stresses are found to be maximum at the pier-pier cap connections.

The strain obtained due to the application of thermal load is shown in Figure 23. Blue indicates compressive strain and red indicates tensile strain.

6.2. Seismic Type (Cyclic Loading) Results. With the application of reverse cyclic load, the following displacement values are obtained as shown in Figure 24. The maximum displacement is found to be 17.76 mm.

The stresses developed due to reverse cyclic loads are as shown in Figure 25. The stresses developed are found to be maximum at the pier-pier cap connections.

The strain values obtained due to the application of seismic load are as displayed in Figure 26. It is found that the corners of the pier-pier cap junction experience maximum strain.

7. Validation and Discussion of Results

The variation of lateral load with respect to lateral displacement as determined from the experimental test was found to be similar to that value obtained from the computational model. The displacement value obtained from the numerical study was less than the experimental value by 9%. This might be due to the assumed perfect bonding between steel and concrete and the perfect fixity condition at the base. In the experimental testing, the specimen adjusts to its position during the initial stages of loading. The rate of loading of the manual hydraulic jack is not constant. This might have resulted in higher displacements during the experimental test. The load displacement variation with thermal load, strain versus load, and load displacement variation for seismic type loading are illustrated in Figures 27 –29, respectively.

The lateral load versus lateral displacement graph shows that the specimen is within the elastic limit and hence the behavior is linear.

From the axial stress versus axial strain graph, the average modulus of elasticity was found to be 32500 MPa, which is similar to the modulus of elasticity as computed by formula 5000 (fck) 0.5 which is around 30414 MPa. The strain measures from the strain gauges at the initial loading

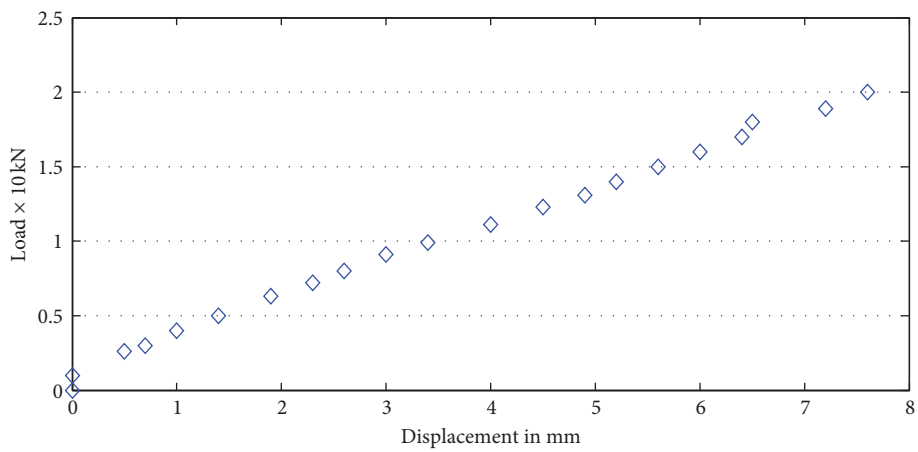

Figure 16: Load versus displacement for the thermal load.

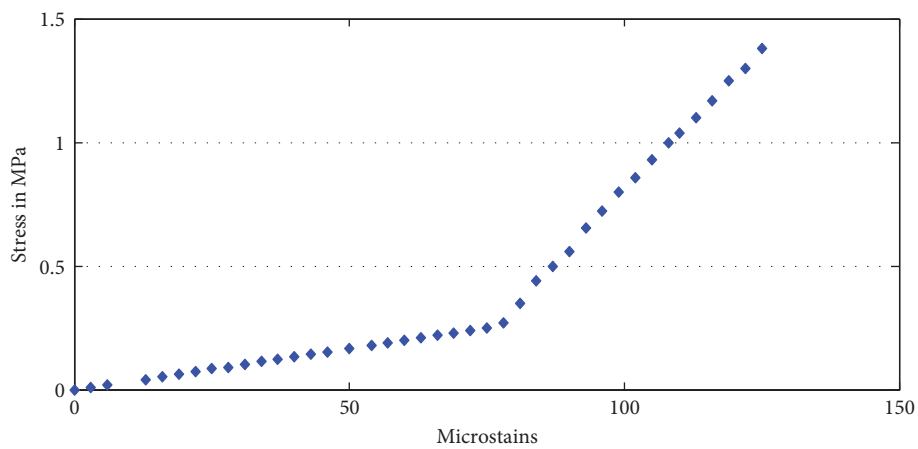

Figure 17: Axial stress versus axial strain (thermal strain at column top).

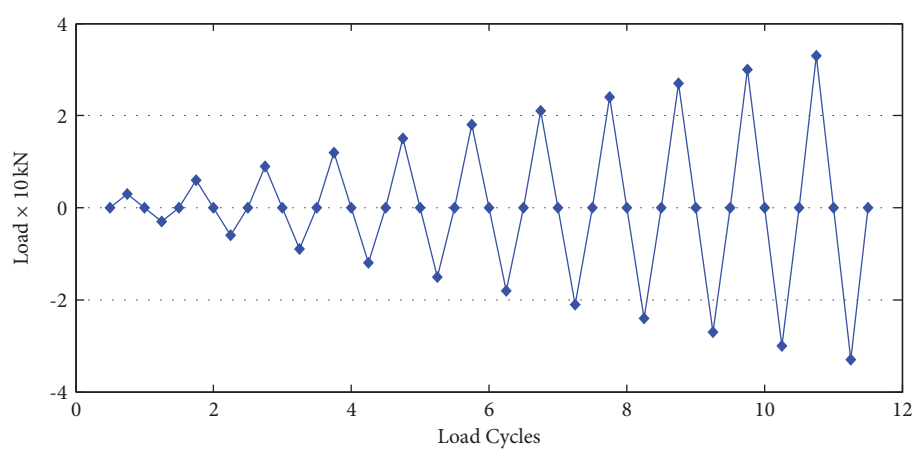

Figure 18: Loading pattern.

stage were irregular. This might have been due to the rearrangement and shape changes of the silicon cover over the strain gauges.

Response of pier-pier cap system subjected to seismic loading.

The load versus displacement curve for experimental tests showed that the specimen is in its elastic state and there is no indication of yielding of the rebars and no cracks were observed. Thus, the structure is safe for the design of seismic load.

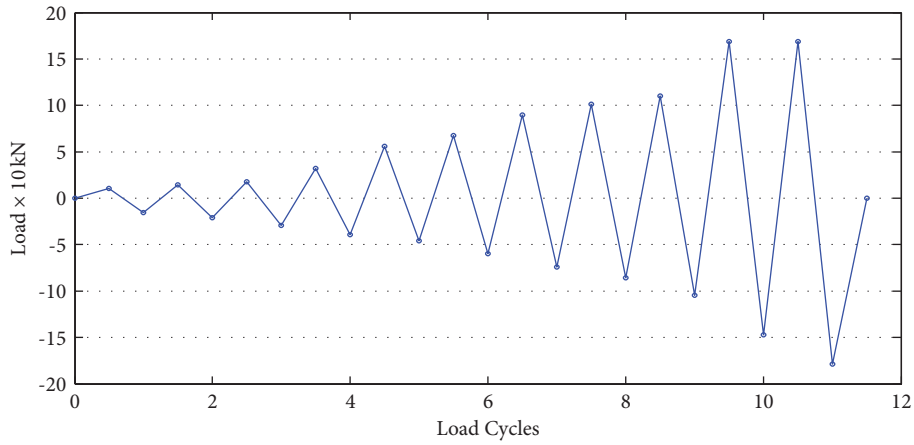

Figure 19: Load cycles.

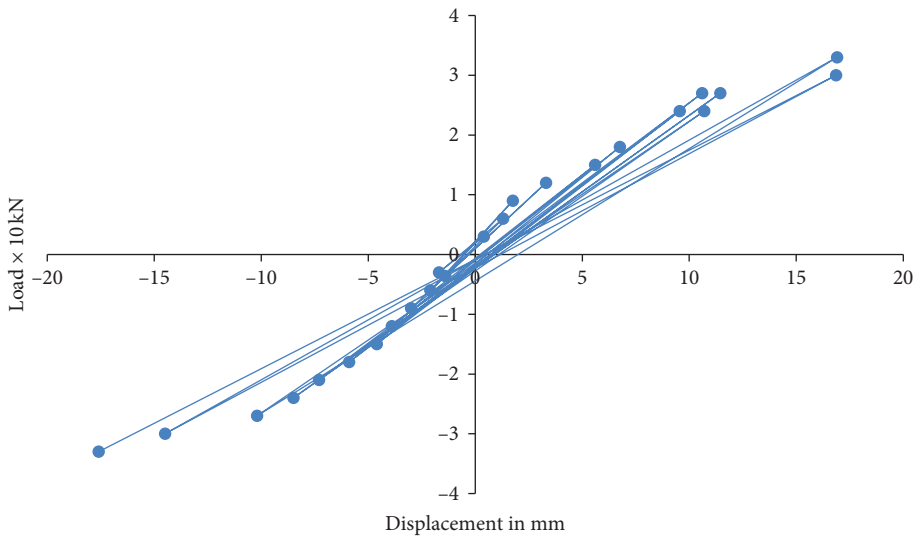

Figure 20: Load displacement graph (experimental test).

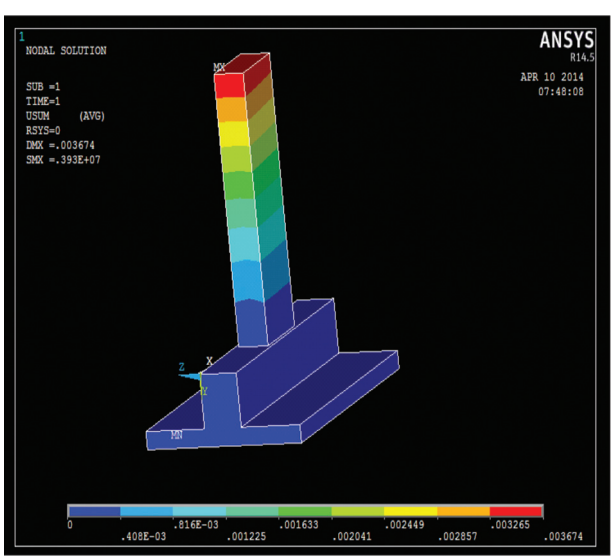

Figure 21: Displacement due to thermal load.

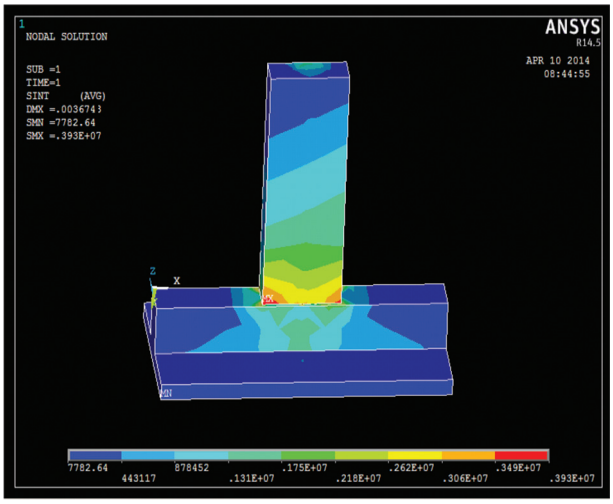

Figure 22: Stresses caused due to thermal load.

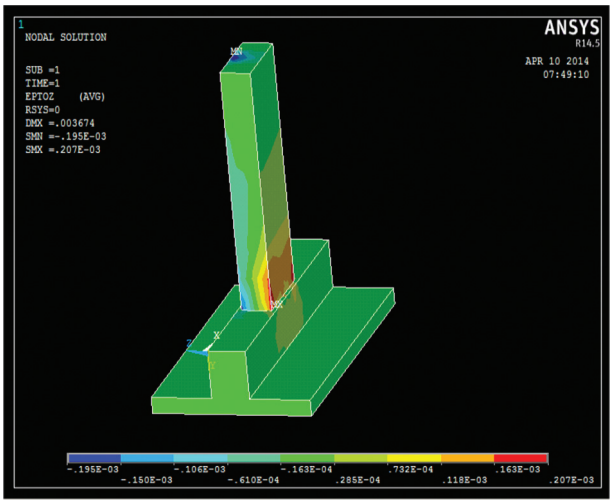

Figure 23: Strains caused due to thermal load.

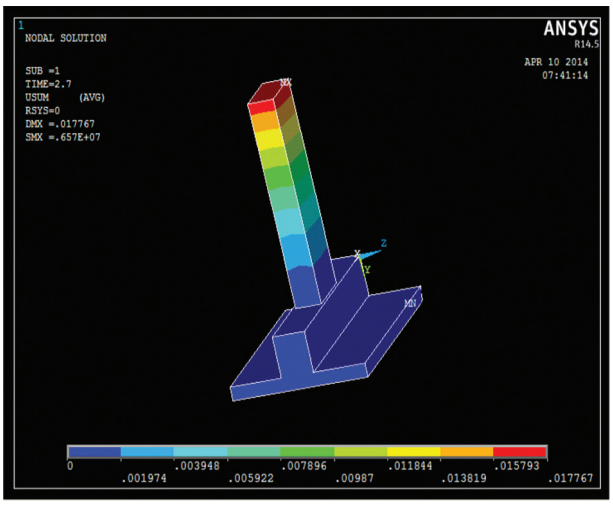

Figure 24: Displacement caused due to seismic loading.

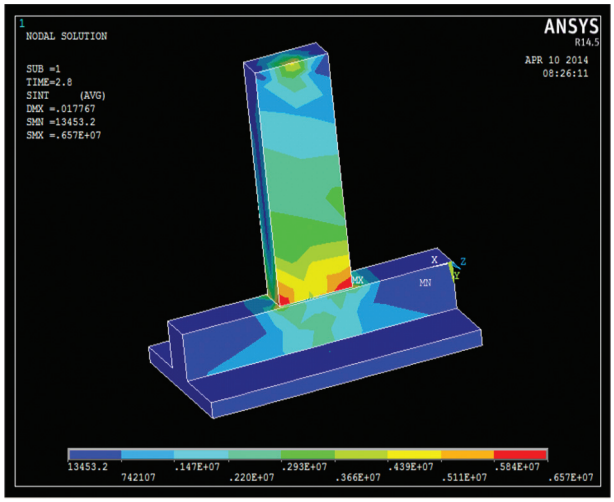

Figure 25: Stresses caused due to seismic loading.

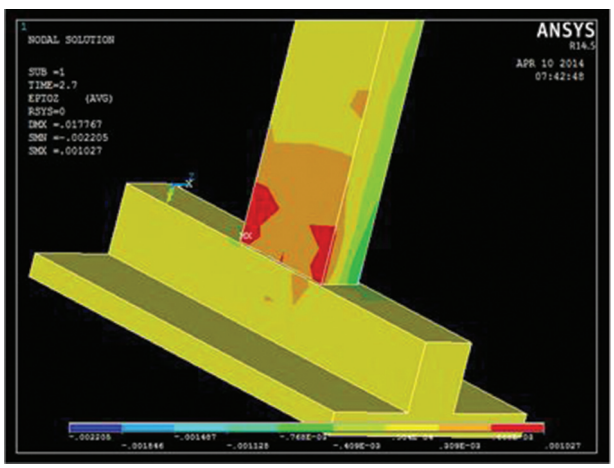

Figure 26: Strain caused due to seismic type loading.

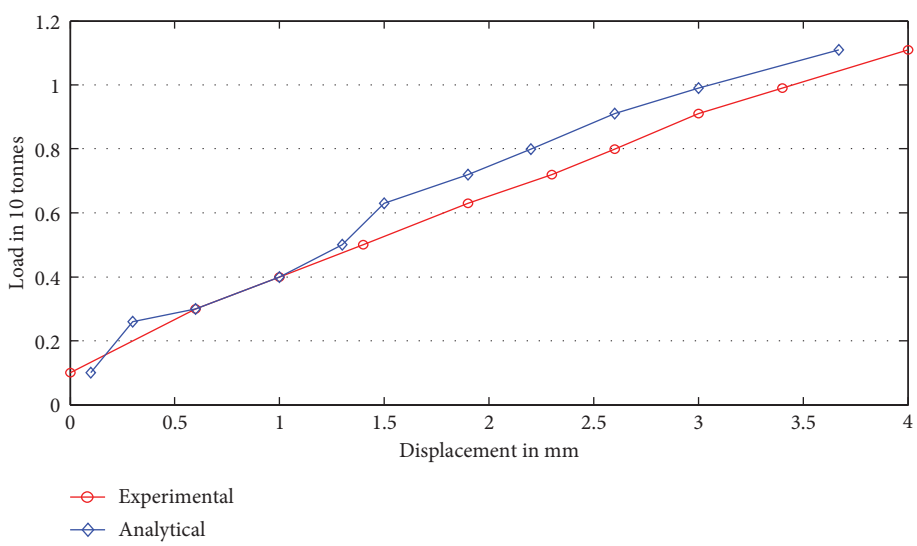

Figure 27: Load displacement variation with thermal load.

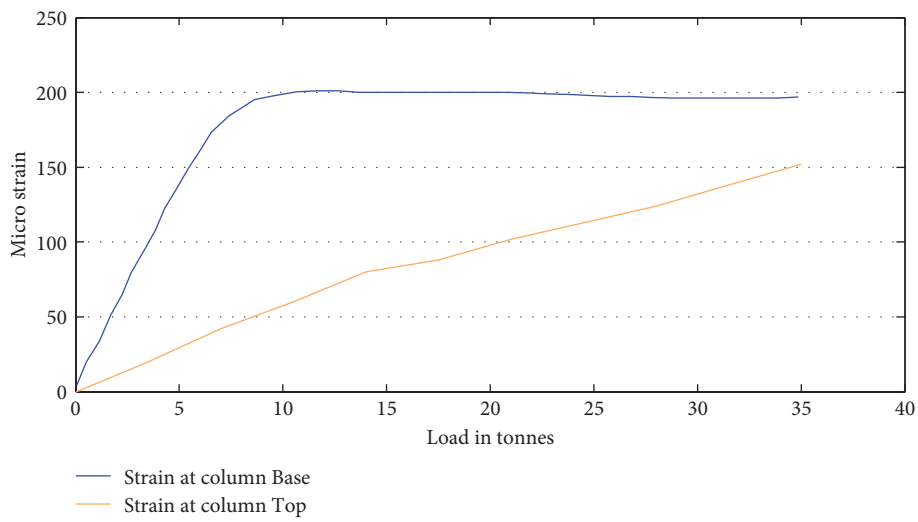

Figure 28: Strain versus load plot.

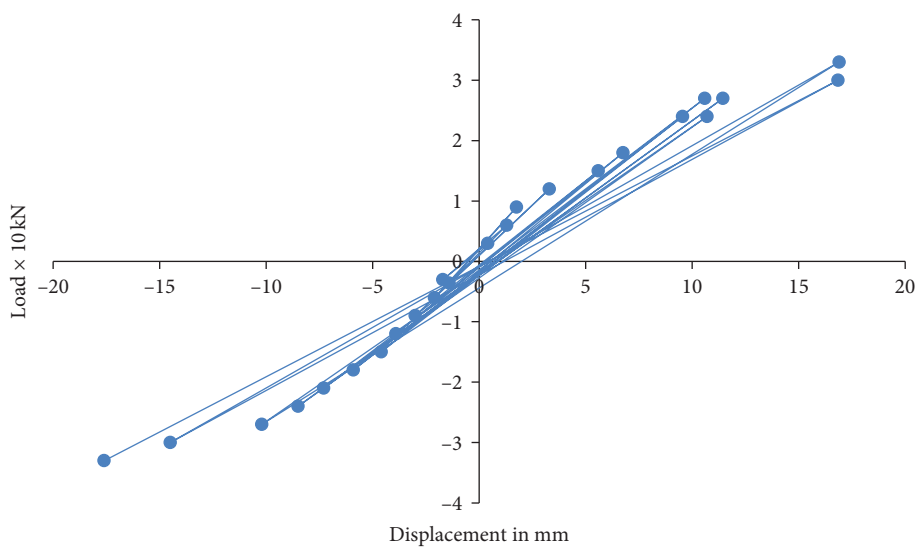

Figure 29: Load displacement variation for seismic type loading.

8. Conclusions

As discussed previously, two ¼ scaled-down models of an integral bridge were considered for the present study. Using the load values obtained from STAAD.Pro, the design and bridge detailing are developed. Based on the material properties, the mix design of concrete was conducted. The reinforcement cage was then prepared on which the strain gauges were fixed. Casting and curing of the specimens were carried out. The specimens were then moved to the strong floor and tested for thermal and seismic loads, respectively. Then the models of the specimens were generated in ANSYS 14.5 and analyzed. The experimental results obtained were validated with the numerical results.

The main novelties of this research were the computational modeling and experimental investigation of pier-pier cap connections. Little research work has been carried out in this context, particularly on this type of connection subjected to thermal and seismic loads.

The following conclusions have been inferred from the study of the behavior of pier-pier cap connections of an integral bridge.

(1) The numerical results were in accordance with the experimental results. The maximum displacements of the experimental tests were found to be higher than the numerical predictions by 9%.

(2) The connection, when subjected to thermal loads, developed stresses in the range of 3–5 MPa which is within the elastic range.

(3) For seismic loads, the stresses developed were about 8 MPa which is also within the elastic limit. The design of the reinforcement is safe for this type of load.

(4) It is observed from the numerical and experimental investigation that the stresses developed at the pier-pier cap connections are much higher than the stresses at the base of the pier.

(5) There was no visual evidence of cracking. The reinforcement provided and the cross section were sufficient for thermal stresses as well as seismic loading. Hence, under service loads, the thermal effect is negligible and the provided section is safe under seismic loads.

Future studies can include further enhancements such as the optimization of the reinforcement area. The scale of the model can be modified as desired. The load can be applied along the transverse direction, and its magnitude with the number of loading cycles can also be modified to investigate the postelastic behavior.

Data Availability

The datasets generated during the current study are available from the corresponding author upon request.

Conflicts of Interest

The authors declare that they have no conflicts of interest.

Acknowledgments

The testing of the specimens was performed at the Structural Testing Laboratory of College of Engineering, Guindy, Anna University, Chennai 25. The authors especially thank professor, Dr. K.P. Jaya and her students for guiding and helping with this research work. S. Avudaiappan and E. I. Saavedra Flores acknowledge funding coming from the Universidad de Santiago de Chile, USACH, Proyecto POSTDOC_DICYT, Código 052018SF_ POSTDOC and Project AP_539SF, Vicerrectoría de Investigación, Desarrollo e Innovación.

References

[1] J. Holombo, M. J. N. Priestley, and F. Seible, "Continuity of precast prestressed sliced-girder bridges under seismic loads," *PCI Journal*, vol. 45, no. 2, pp. 40–63, 2000.

[2] W. G. Wassef, C. Smith, C. M. Clancy, and M. J. Smith, *Comprehensive Design Example for Pre-stressed Concrete Girder Superstructure Bridge with Commentary*, Federal Highway Department, Harrisburg, Pennsylvania, 2003.

[3] R. E. Abendroth and L. F. Greimann, "Field testing of integral abutments," Iowa State University, Final Report, 2005.

[4] A. Panday and M. Tandon, "Integral flyovers in Delhi," *Indian Concrete Journal*, vol. 79, 2005.

[5] P. Laman, "Thermally induced superstructure stresses in prestressed girder integral abutment bridges," in *Proceeding of the 6th International Bridge Engineering Conference*, Journal of the Transportation Research Board, National Research Council, Washington, DC, USA, July 2005.

[6] E. Rodriguez Leo, "Temperature effects on integral abutment bridges for the long-term bridge performance program," All Graduate Thesis and Dissertations, 2011.

[7] H. G. Russell and L. J. Gerken, "Jointless bridges - the knowns and the unknowns," *ACI – Concrete International*, vol. 16, pp. 44–48, 1994.

[8] X. Chen, Z. Guan, J. Li, B. F. Spencer Jr., and F. Asce, "Shake table tests of tall-pier bridges to evaluate seismic performance," *Journal of Bridge Engineering*, vol. 23, no. 9, Article ID 04018058, 2018.

[9] S. A. Mitoulis, "Challenges and opportunities for application of integral abutment bridges in earthquake prone areas: a review," *Soil Dynamics and Earthquake Engineering*, vol. 135, Article ID 106183, 2020.

[10] S. Argyroudis, A. Palaiochorinou, S. Mitoulis, and D. Pitilakis, "Use of rubberised backfills for improving the seismic response of integral abutment bridges," *Bulletin of Earthquake Engineering*, vol. 14, no. 12, pp. 3573–3590, 2016.

[11] S. Sritharan, J. Vander Werff, and R. Snyder, *Use of Precast I-Girders for Accelerated Bridge Construction in High Seismic Regions*, US-Japan Bridge Engineering Workshop, Tsukuba, Japan, 2011.

[12] R. Wang, B. Ma, and Xu Chen, "Seismic performance of prefabricated segmental bridge pier with grouted splice sleeve connections," *Engineering Structures*, vol. 229, Article ID 111668, 2021.

[13] J. Jia, K. Zhang, M. Saiid Saiidi et al., "Seismic evaluation of precast bridge columns with built in elastomeric pads," *Soil Dynamics and Earthquake Engineering*, vol. 128, Article ID 105868, 2020.

[14] B. Zakeri and F. Zareian, "Design of Bridges with skewed abutments for a target tolerable seismic loss," *Engineering Structures*, vol. 164, pp. 325–334, 2018.

[15] The Design of Integral Bridges, "BA 42/96, amendment No.1," *Design Manual for Roads and Bridges*, vol. 1, 2003 Section 3, Part 12.

[16] 2020 Specifications refer to the current AASHTO LRFD Bridge Design Specifications and current VDOT Modifications (IIM-S&B-80), File No. 15. TOC-3.

[17] M. Arockiasamy, N. Butrieng, and M. Sivakumar, "State-of-the-art of integral abutment bridges: design and practice," *Journal of Bridge Engineering*, vol. 9, no. 5, 2004.

[18] S. Arsoy, R. M. Barker, and J. M. Duncan, "The behavior of integral abutment bridges," Final Contract Report VTRC 00-CR3, Virginia Transportation Research Council, Charlottesville, Virginia, 1999.

[19] Indian Roads Congress, Irc:6, *Standard Specification and Code of Practice for Road Bridges*, Loads and stresses, New Delhi, India, Section: II edition, 2010.

[20] Indian Standard, IS 10262, *Concrete Mix Proportions Guidelines*, First Revision Bureau of Indian standards, New Delhi, India, 2009.

[21] S. Greeshma, K. P. Jaya, and S. L. Annilet, "Analysis of flanged shear wall using ANSYS concrete model," *International Journal of Civil and Structural Engineering*, vol. 2, no. 2, pp. 454–465, 2011.

[22] S. Greeshma, C. Rajesh, and K. P. Jaya, "Seismic behavior of shear wall-slab joint under lateral cyclic loading," *Asian Journal of Civil Engineering*, vol. 13, no. 4, pp. 455–464, 2012.

[23] S. Bhavik Rameshchandra, "3D finite element analysis of integral abutment bridges subjected to thermal loading," M. E. thesis, Kansas State University Manhattan, Kansas, 2007.

[24] Indian Standard, IS 456, *Plain and Reinforced Concrete*, 2000.

[25] Indian Standard, IS 1893, *Earthquake Resistant Design of Structures*, PHI Learning Private Limited, New Delhi, India, 2002.